

Article

Input-Shaped Model Reference Control Using Sliding Mode Design for Sway Suppression of An Industrial Overhead Crane

Nattapong Suksabai^a and Ittichote Chuckpaiwong^{b,*}

Department of Mechanical Engineering, Faculty of Engineering, Mahidol University, 999 Phutthamonthon 4 Rd., Salaya, Nakhon Pathom 73170, Thailand

E-mail: ^anattapong.nup@gmail.com, ^{b,*}ittichote.chu@mahidol.ac.th (Corresponding author)

Abstract. Input-shaped model reference control using sliding mode design is a proven method for controlling systems with parameter variations and disturbance. However, this method has never been reported for an industrial overhead crane, which is operated under nonlinear elements such as acceleration and deceleration limits caused by inverters for driving a crane in speed control mode. The successful implementation of this method will allow the crane to be operated in “hybrid mode”, which results in the fastest response from the feedforward control technique, unity magnitude zero vibration (UMZV) and tracking performance from the feedback control. This paper shows the implementation and experimental result of the input-shaped model reference control using sliding mode design for sway suppression of an industrial overhead crane. The control scheme was implemented on an industrial grade 1-ton overhead crane using a PLC and inverters. The experiments compared the control results of the UMZV and the presented control scheme on the industrial overhead crane in the cases that the system parameters are known and uncertain. When the parameters are uncertain, the presented method, with the feedback elements, provided the advantage of reducing residual vibration, while keeping the benefits of the UMZV performance.

Keywords: Overhead crane, sway suppression, rate limiter, input shaping, model reference control.

ENGINEERING JOURNAL Volume 27 Issue 2

Received 3 May 2022

Accepted 21 February 2023

Published 28 February 2023

Online at <https://engj.org/>

DOI:10.4186/ej.2023.27.2.1

1. Introduction

A payload that attached under the crane will be oscillated due to an arbitrary motion of an overhead crane. The oscillating nature of the crane makes it difficult to navigate the payload manually, and often leads to unexpected crashing. Many researches on sway suppression were proposed, which are reviewed in [1]. Several feedforward control and feedback control schemes since 2000 to 2016 were included. All the techniques successfully obtained sway suppression including input shaping techniques, command smoothing techniques, linear controls, non-linear controls, intelligent controls, and adaptive controls.

Among those techniques, input shaping and command smoothing are considered feedforward controls, which require no sway feedback sensors. After 2016, feedforward controls for crane applications were further developed to improve sway suppression performance. Maghsoudi and Mohamed [2] implemented the distributed delay input shaping on an overhead crane, which was originally invented by Vyhli' dal [3] and is more robust than the conventional input shaping. Viet Duc La and Kien Trong Nguyen [4] combined feedforward input shaping with a passive control called radial spring-damper for sway suppression of a boom crane. The experiment on the lab-scale boom crane was carried out and successful results were obtained. Mohammed A, Alghanim K [5] proposed the novel input shaping technique called an adjustable Zero Vibration for overhead cranes. The final design showed that the input shaper generated step inputs, which was a suitable acceleration profile. AbdulAziz Al-Fadhli and Emad Khorshid [6] proposed a new technique using Bezier trajectory generator for sway suppression. Besides input shaping, command smoothing is an alternative technique, which shows promising performance in recent studies. In one study, a command smoother designed by signal decomposition was implemented on an overhead crane. The parameters of the command smoother were offline calculated using linear regression analysis. It resulted that the overhead crane parameters were not needed in the design process and the technique still provides good sway suppression [7]. Later, an online version of the command smoother was developed for countering parameter variation and disturbance situations. It is similar to feedback controls, which directly compensate the signal input by the signal output, but instead the signal output is used for online parameter estimation, making the command smoother being adaptive. The result indicates that the new proposed technique provided more robustness properties than an offline version [8].

Many feedback controls for crane applications were improved as well, especially with sliding mode controls, which have ability for dealing with system parameter variation and disturbances. Biao Lu and Yongchun Fang [9] designed a sliding mode control for crane position and sway control, in which the overhead crane was considered as an underactuated system. The design control scheme

proved that it could counter both matched and unmatched disturbance. A matched disturbance was observed by a disturbance observer and an unmatched disturbance was bounded at a given limit. Then the control scheme used both disturbance values for designing the control law. Later, Xiutao Gu, and Weimin Xu [10] used A novel time-varying extended state observer (ESO) to lump the matched and unmatched disturbances without requiring the upper limit of the disturbances. Then the observed variable is used to compensate the real disturbances in the overhead crane system, which is based on the moving sliding surface design and shattering-free control law. Viet-Anh Le, Hai-Xuan Le, Linh Nguyen, and Minh-Xuan Phan [11] investigated adaptive hierarchical sliding mode control for 2D overhead crane for controlling crane position and sway angle, in which a fuzzy observer was used for estimating disturbance and uncertain parameters. The similar results can be observed in [12], which used a neural network instead of a fuzzy observer. In general feedback controls, the disturbance and uncertain parameters can be approximated by some kinds of estimators, making the overhead crane being controlled and stability guaranteed. Another sliding mode control design for an overhead crane can be found in [13], where adaptive version with three layers of sliding surface covering all system states of double pendulum system was presented. Lately, three layers of sliding surfaces form using the fuzzy logic as the adaptive mechanism was exploited for the 6 degrees of freedom overhead crane, where the elasticity of the hoisting cable effect was considered. The highly promising results were obtained through mathematical model simulation [14]. However, uncomplicated version of the sliding mode control was presented where the two controllers were combined, coupling PD controller with sliding model control was proposed for an overhead crane considered as double pendulum system [15]. The control equivalent parts of sliding mode control were replaced by a PD controller. The stability performance of the system was also analyzed.

The advantages and disadvantages of feedforward and feedback controls are contrary to each other. Combining their advantages would improve a control system performance. However, combining feedback and feedforward controls in series may improve sway suppression of the overhead crane system, but with a degraded transient response. By doing so, the feedback control works like a regulator trying to bring the sway angle to zero, which may disturb the control signal from the feedforward by extending the control signal duration. To fix this problem, the feedback control must control the actual sway angle to track the desired trajectory provided by the feedforward control. One of the established methods to track the desired trajectory is a model reference control, which requires rough knowledge of the system dynamic. Some model reference controls will be reviewed here. Abdullahi A.M., et al. [16] combined adaptive command smoother and integral sliding mode control for sway suppression of an overhead crane using fully 3D dynamic model as a reference model. The

experimental result showed that the proposed control scheme has ability to counter external disturbance and system parameter variation. Another result expressed that the feedforward control mechanism reduces chattering on control signal as well as reduces control afford. It also reduces maximum sway angle during motions. The same result can be observed from another paper [17], where zero vibration (ZV) input shaping was combined with the model reference control. However, other research on a double pendulum of an overhead crane using a single pendulum as the model reference was reported in [18-20]. The results also emphasize that combining feedforward and feedback control in a model reference form can be used for disturbance rejection, parameter variation, and reducing control afford. Lately, a command smoother as the reference model was combined with a PID controller for sway suppression of a double pendulum overhead crane, where the controller parameters were optimized from the nonlinear dynamic model simulation [21]. Finally, a given first-order system as the reference model was used for trajectory tracking control performed by a moving sliding mode design. The model reference form is expected for improving the following performances: non-overshoot, fast convergence rate, short settling time [22].

All evidence emphasizes that the model reference control that combines feedback and feedforward is suitable for overhead crane applications. The sliding mode design has a powerful ability for parameter variation and disturbance situations due to the nonlinear switching element term and model-based design. However, input-shaped model reference control using sliding mode control design has never been reported for an industrial overhead crane that is operated under nonlinear elements such as acceleration and deceleration limits caused by the inverters for driving the crane in speed control mode. However, this control type has already proved its performance for tracking and disturbance rejection ability in small cranes without considering hardware limitations [16]. Therefore, this work will present the implementation of the input-shaped model reference control using sliding mode design on an industrial overhead crane, which certainly benefits crane engineers for developing sway suppression in practice. Experimental results will be provided to show the sway suppression performance and corresponding transient response using the selected input shaper, unity magnitude zero vibration input shaper (UMZV). It is expected to move the crane with minimal payload sways by means of the fastest input shaper control scheme. Meanwhile, the input shaper and the referenced dynamic model are used as the trajectory generator for the feedback mechanism to correct the input shaper signal when disturbance or parameter uncertainty occurred.

The rest of this paper organizes as follows. A dynamic model of the overhead crane is derived in Section 2 for the controller design. Control design method is stated in Section 3, where UMZV input shaper is briefed, and the derivation of the model reference control based on sliding mode control is provided. Section 4 shows simulation and

experimental result of this implementation. Finally, the conclusion is provided in Section 5.

2. Dynamic Model

An industrial overhead crane is sufficiently considered as a single pendulum (payload) attached under a moving part (trolley). In Fig. 1, the trolley mass (m_t) moves forward from rest in x direction where x is the trolley displacement. The payload mass (m) at the chain length (l) is considered a simple pendulum when the payload sway angle is θ , and the payload displacement is x_p . Figure 1 demonstrates schematic diagram of the overhead crane in one dimension. A dynamic model of the overhead crane is developed by formulating the kinetic energy and the potential energy of the system, which are

$$\begin{cases} T = \frac{1}{2}(m_t \dot{x}^2) + \frac{1}{2}m(\dot{x}_p^2) \\ V = mgl(1 - \cos\theta) \end{cases} \quad (1)$$

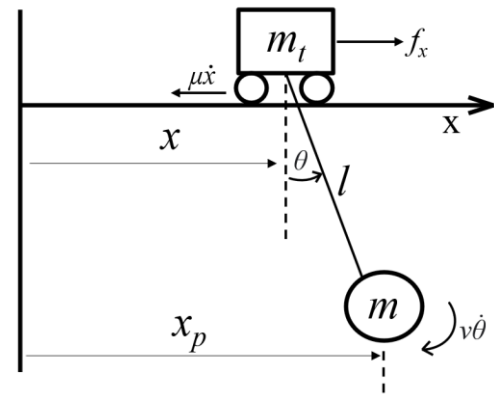


Fig. 1. Free body diagram of the single-pendulum overhead crane.

From the Fig. 1, the payload displacement in x -axis is obtained by:

$$x_p = x + l \sin\theta \quad (2)$$

Taking a time derivative to Eq. (2) yields the payload velocity as follows

$$\dot{x}_p = \dot{x} + l\dot{\theta} \cos\theta \quad (3)$$

Taking a square to Eq. (3) yields a squared payload velocity as shown below

$$\dot{x}_p^2 = \dot{x}^2 + 2x\dot{\theta} \cos\theta + l^2\dot{\theta}^2 \cos^2\theta \quad (4)$$

Letting $\cos^2\theta = 1$, Eq. (4) is simplified to

$$\dot{x}_p^2 = \dot{x}^2 + 2x\dot{\theta} \cos\theta + l^2\dot{\theta}^2 \quad (5)$$

To synthesize a dynamic model of the overhead crane, the Lagrange's equations are considered, one for generalized coordinate x ,

$$\frac{d}{dt} \left(\frac{L}{\dot{x}} \right) - \frac{L}{x} = f_x - \mu \dot{x} \quad (6)$$

and another one for generalized coordinate θ .

$$\frac{d}{dt} \left(\frac{L}{\dot{\theta}} \right) - \frac{L}{\theta} = -v\dot{\theta} \quad (7)$$

The left-hand sides of the Lagrange's equations are considered as conservative energy, described by the Lagrange function (L) that relates to those kinetic and potential energies ($L = T - V$). Meanwhile, the right-hand sides are for the generalized forces for each coordinate where f_x is the actuated force acting on the trolley for moving in the x direction, $\mu \dot{x}$ is the trolley wheel's friction, and $v\dot{\theta}$ is the viscosity torque that slightly damps the payload oscillation. The Lagrange function is expressed as

$$L = T - V = \frac{1}{2} (m_t \dot{x}^2) + \frac{1}{2} m (\dot{x}^2 + 2\dot{x}l\dot{\theta} \cos \theta + l^2 \dot{\theta}^2) - mgl(1 - \cos \theta) \quad (8)$$

By substituting Eq. (8) into Eq. (6), the dynamic model of overhead crane is obtained as Eq. (9), which described relation of the actuator force (f_x) and the trolley acceleration. Other forces are considered as disturbances which are the sway reaction force and the wheel's friction force.

$$(m_t + m) \ddot{x} + ml\ddot{\theta} \cos \theta - ml\dot{\theta}^2 \sin \theta = f_x - \mu \dot{x} \quad (9)$$

Substituting Eq. (8) into Eq. (7) yields Eq. (10), which described relation of the trolley acceleration and the payload angular acceleration.

$$m\ddot{x} \cos \theta + ml^2 \ddot{\theta} + mgl \sin \theta = -v\dot{\theta} \quad (10)$$

By linearizing Eq. (10), the transfer function that describes the payload sway and the trolley acceleration is expressed in Eq. (11). Where $b_0 = v/ml^2$ is introduced for simplifying the dynamic viscosity term. The bode plot was illustrated in literature, which indicated that b_0 can be sufficiently approximated in practice [23].

$$\frac{\theta}{\ddot{x}} = \frac{-1/l}{s^2 + b_0 s + g/l} \quad (11)$$

However, for an industrial overhead crane, controlling the trolley by mean of the actuated force (f_x) is unusual. Each AC induction motor on an overhead crane is usually driven by an inverter that operates under speed control mode. To move the trolley within a maximum velocity limit of the crane, only the velocity command is needed. Any desired velocities within a bounded range will be achieved under a limited rate of change (acceleration and deceleration limits). All disturbance forces including sway reaction force and friction force in Eq. (9) can be neglected. Therefore, only Eq. (10) is required for the dynamic equation in our work.

Since the inverter introduces a dynamic behaviour between the trolley velocity and the velocity command, the dynamic model must be derived. An empirical model that describes relation between the trolley velocity (\dot{x}) and the velocity command (u) was proposed by Sorensen and Singhose [24] and was then verified by the authors [25]. Eq. (12) expresses kinematic equation of the trolley when u is the velocity command and q is a nonlinear positive uncertain value, which depends on the acceleration and deceleration limits or even jerk effect with respect to the inverter settings. Note that a similar idea can be found in Mori M and Tagawa Y's work [26], where a robust sway control design was successfully obtained.

$$\ddot{x} + q\dot{x} = qu \quad (12)$$

The transfer function form of Eq. (12), called the driven unit model, is expressed as follows:

$$\frac{\dot{x}}{u} = \frac{q}{s + q} \quad (13)$$

To accommodate the use of trolley velocity in speed control mode of an inverter, the transfer function of the pendulum model in Eq. (11) is slightly changed to

$$\frac{\theta}{\dot{x}} = \frac{-1/l^s}{s^2 + b_0 s + g/l} \quad (14)$$

The driven unit model in the Eq. (13) and the pendulum model in Eq. (14) will be used for the controller design using input-shaped model reference control.

3. Control Method

3.1 Input Shaping Using UMZV Technique

A vibrated system can be turned to a well damped system by applying an input shaping technique, where an original signal is convoluted by a sequence of impulses. The new shape of the original signal will extinguish the system vibration. While the obvious benefit of the input shaping is vibration suppression, the major drawback is that the transient response will be extended. The unity magnitude zero vibration (UMZV) is one of the well-known input shaping techniques, which is used to eliminate residual vibration of oscillated systems with optimal transient response. In UMZV, the four constraints are considered including residual vibration constraint, amplitude constraint, initial time constraint and number of impulses. The residual vibration constraint was considered as the amplitude ratio between the vibration response from multi-impulse A_Σ (shaped input) and the vibration response from a single impulse A_1 (unshaped input), which is expressed in Eq. (15) as

$$V(\omega, \zeta) = \frac{A_\Sigma}{A_1} = e^{-\zeta \omega t} \sqrt{[C(\omega, \zeta)]^2 + [S(\omega, \zeta)]^2} \quad (15)$$

where $C(\omega, \zeta)$ and $S(\omega, \zeta)$ are cosine and sine functions, respectively, as obtained below:

$$\begin{cases} C(\omega, \zeta) = \sum_{i=1}^n A_i e^{\zeta \omega t_i} \cos(\omega \sqrt{1-\zeta^2} t_i) \\ S(\omega, \zeta) = \sum_{i=1}^n A_i e^{\zeta \omega t_i} \sin(\omega \sqrt{1-\zeta^2} t_i) \end{cases} \quad (16)$$

Certainly, ω and ζ are the natural frequency and the damping ratio of the oscillated system, respectively. t_i is the time location of each impulse, and A_i is the impulse amplitude. $V(\omega, \zeta)$ is the percentage of vibration, which is set to zero to find the impulse amplitude and time location (that is why it is called zero vibration). The second constraint is considered an amplitude constraint. This constraint prevents the shaped signal amplitude to not exceed its original maximum value. Eq. (17) expresses the amplitude constraint as

$$\sum_{i=1}^n A_i = 1 \text{ where } A_i = (-1)^{i+1} \quad (17)$$

where n is the number of impulses. In UMZV design, n is set to 3. By defining the impulse amplitude constraint and the number of impulses, the amplitudes of the 3 impulses are 1, -1, and 1 respectively. The rest is to find the period time between these impulses. The initial time constraint is set that the time location of the first impulse is zero, $t_1 = 0$. The time locations of the second and third impulses, t_2 and t_3 , are left for finding. According to the residual vibration constraint that Eq. (15) is set to zero, the cosine and sine functions in Eq. (16) must be set to zero as well. Substituting A_1, A_2, A_3, t_1, t_2 and t_3 into Eq. (16), and setting it to zero, the new equations are obtained in the Eq. (18) as follows:

$$\begin{cases} 1 - e^{\zeta \omega t_2} \cos(\omega \sqrt{1-\zeta^2} t_2) + e^{\zeta \omega t_3} \cos(\omega \sqrt{1-\zeta^2} t_3) = 0 \\ 0 - e^{\zeta \omega t_2} \sin(\omega \sqrt{1-\zeta^2} t_2) + e^{\zeta \omega t_3} \sin(\omega \sqrt{1-\zeta^2} t_3) = 0 \end{cases} \quad (18)$$

However, for a damped system (ζ is greater than zero), t_2 and t_3 cannot be analytically solved. To fix this problem, undamped system (ζ is zero) is initially considered, and the locations of the second and the third impulses can be solved as shown below:

$$t_2 = \frac{\pi}{3\omega}, t_3 = \frac{2\pi}{3\omega} \quad (19)$$

Singhose, Seering, and Singer [27] proposed a solution of UMZV for a damped system where the damping ratio was between 0 to 0.35. A polynomial cubic form, which is a function of the damping ratio, was used for correcting t_2 and t_3 of the undamped system as shown in Eq. (20)

$$\begin{bmatrix} t_2 \\ t_3 \end{bmatrix} = \frac{2\pi}{\omega} \begin{bmatrix} 0.16704 & 0.27242 & 0.20345 & 0 \\ 0.33323 & 0.00533 & 0.17914 & 0.20125 \end{bmatrix} \begin{bmatrix} 1 \\ \zeta^1 \\ \zeta^2 \\ \zeta^3 \end{bmatrix} \quad (20)$$

where the natural frequency and the damping ratio can be calculated from the payload model parameters as follows:

$$\begin{cases} \omega = \sqrt{g/l} \\ \zeta = \frac{b_0}{2\omega} \end{cases} \quad (21)$$

However, for damping ratio from 0.01 to 0.9, UMZV can be calculated by the proposed equations in [28].

The UMZV described above still cannot be used with the industrial overhead crane system because some nonlinear elements exist. Although, the relation between the payload sway angle and the trolley velocity can be approximately modelled by a second order linear system, the trolley velocity and the velocity command are modelled as the nonlinear system containing acceleration and deceleration limits, denoted by a nonlinear positive uncertain value (q) in Eq. (13). To avoid nonlinear effects of the acceleration and deceleration limits, Sorensen and Singhose [20] suggested a rate limiter to limit rate of changes of a reference signal before sending to the input shaper. The trolley is then moved according to the shaped signal within the rate limit settings in the inverter. Later, Piedrafita, and Comín [29] used gaussian filter for smoothing a reference signal for the same purpose. In this work, a UMZV input shaper was incorporated with a rate limiter where the referenced velocity (v_r) was sent to the rate limiter (the filter) first before sending to the input shaper. In any forms, the rate limiter prevents rate of change of the referenced velocity from exceeding the acceleration and deceleration limits of the inverter in the driven unit. Then the rate-limited velocity (v_{limit}) was passed to the UMZV input shaper for vibration cancellation, as depicted in Fig. 2. Figure 3 demonstrates an example of signal convolution of the UMZV input shaper.

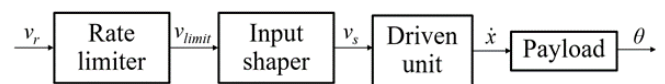


Fig. 2. Sway suppression model of the input shaper and rate limiter for an industrial overhead crane.

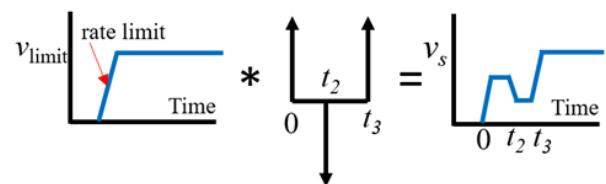


Fig. 3. Example of the convolution of the rate-limited step-input signal in the UMZV input shaper.

Eq. (22) expresses a rate limiter, which is modelled by a constant of acceleration limit (A) and the deceleration limit (D) in the continuous form.

$$\dot{v}_{limit} = \begin{cases} A, \dot{v}_r > A \\ D, \dot{v}_r < D \\ \dot{v}_r, D < \dot{v}_r < A \end{cases} \quad (22)$$

3.2 Input-Shaped Model Reference Control

To enhance effectiveness of the input shaping in the presence of disturbance and parameter variation, a model reference control, also called hybrid feedback control, was used. The input-shaped model reference control, as shown in Fig. 4, contains 3 main blocks: a reference model, an observer, and a controller. By making the reference model and the state observer similar to the plant (the crane system), the feedback and the feedforward controls ideally work together for sway suppression with no conflict. In the other words, while the crane system is operated, the reference model is parallely calculated for comparing system states. When the crane system reaches the desired condition, both system state and reference state are ideally equal according to the approximate parameters of the reference model and the state observer at the desired condition. In this case, the feedback control signal does not contribute to the overall control signal. However, when the crane is operated at a different condition from the desire (such as in a presence of disturbance or model mismatch), the feedback control signal is active for correcting the feedforward signal, making the crane system becomes close to the reference model.

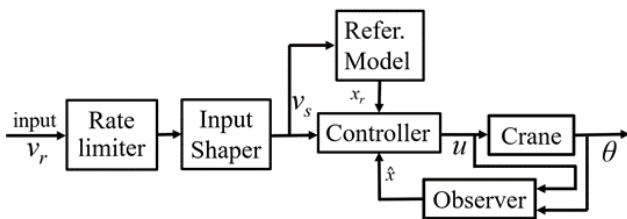


Fig. 4. Diagram of the input-shaped model reference control.

The driven unit model and the pendulum model in Eq. (13) and (14) are used for designing the feedback control. The multiplication of both equations expresses the transfer function when the input is the velocity command, and the output is the payload sway angle.

$$\frac{\theta}{u} = \frac{-\frac{g}{l}s}{s^3 + (q + b_0)s^2 + \left(\frac{g}{l} + qb_0\right)s + q\frac{g}{l}} \quad (23)$$

The dynamic model of the overhead crane in Eq. (23) is described by a state-space controllable canonical form in Eq. (24), where x is a state vector of x_1, x_2 , and x_3 , u is the input control signal, and θ is the output sway angle.

$$\begin{cases} \begin{bmatrix} \dot{x}_1 \\ \dot{x}_2 \\ \dot{x}_3 \end{bmatrix} = \begin{bmatrix} 0 & 1 & 0 \\ 0 & 0 & 1 \\ -a_1 & -a_2 & -a_3 \end{bmatrix} \begin{bmatrix} x_1 \\ x_2 \\ x_3 \end{bmatrix} + \begin{bmatrix} 0 \\ 0 \\ 1 \end{bmatrix} u, \\ \theta = \begin{bmatrix} 0 & -c_2 & 0 \end{bmatrix} \begin{bmatrix} x_1 \\ x_2 \\ x_3 \end{bmatrix} \end{cases} \quad (24)$$

The constants in the state matrix and the output matrix are defined for the system parameters of the controlled system, which are shown as follows:

$$\begin{cases} a_1 = q\frac{g}{l} \\ a_2 = \frac{g}{l} + qb_0 \\ a_3 = q + b_0 \\ c_2 = \frac{g}{l} \end{cases} \quad (25)$$

The reference model can be computed similarly to the crane model in Eq. (24) and (25), except using approximate parameters as shown in Eq. (26). For the driven unit model, the nonlinear value (g) is approximated to be a constant \hat{g} . For the pendulum model, the chain length (l) and the dynamic viscosity (b_0), are fixed at the operating condition. The parameters of the reference model are constants, therefore, the reference model of the industrial overhead crane is a linear system, where the input is the shaped velocity v_s and the output is the desired sway angle θ_r .

$$\begin{cases} \begin{bmatrix} \dot{x}_{r,1} \\ \dot{x}_{r,2} \\ \dot{x}_{r,3} \end{bmatrix} = \begin{bmatrix} 0 & 1 & 0 \\ 0 & 0 & 1 \\ -\hat{a}_1 & -\hat{a}_2 & -\hat{a}_3 \end{bmatrix} \begin{bmatrix} x_{r,1} \\ x_{r,2} \\ x_{r,3} \end{bmatrix} + \begin{bmatrix} 0 \\ 0 \\ 1 \end{bmatrix} v_s, \\ \theta_r = \begin{bmatrix} 0 & -\hat{c}_2 & 0 \end{bmatrix} \begin{bmatrix} x_{r,1} \\ x_{r,2} \\ x_{r,3} \end{bmatrix} \end{cases} \quad (26)$$

Like the crane model, the constants in the reference model are defined for the system parameters of the reference model, denoted by the hat symbol, which are shown as follows:

$$\begin{cases} \hat{a}_1 = \hat{g}\frac{g}{l} \\ \hat{a}_2 = \frac{g}{l} + \hat{g}\hat{b}_0 \\ \hat{a}_3 = \hat{g} + \hat{b}_0 \\ \hat{c}_2 = \frac{\hat{g}}{l} \end{cases} \quad (27)$$

According to the parameter approximation, the true parameters of the controlled system are modelled by the summation of the constant estimations and the approximate-parameter errors as follows:

$$\begin{cases} a_1 = \hat{a}_1 + \Delta\hat{a}_1 \\ a_2 = \hat{a}_2 + \Delta\hat{a}_2 \\ a_3 = \hat{a}_3 + \Delta\hat{a}_3 \\ c_2 = \hat{c}_2 + \Delta\hat{c}_2 \end{cases} \quad (28)$$

To design the feedback control law, sliding mode control was proposed for designing state tracking control. The state errors are defined as

$$\begin{cases} e_1 = x_{r,1} - x_1 \\ e_2 = x_{r,2} - x_2 \\ e_3 = x_{r,3} - x_3 \end{cases} \quad (29)$$

Taking time derivative of the state errors, then substituting Eq. (24) and (26), yields

$$\begin{cases} \dot{e}_1 = e_2 \\ \dot{e}_2 = e_3 \\ \dot{e}_3 = -\hat{a}_1 e_1 - \hat{a}_2 e_2 - \hat{a}_3 e_3 \\ + \Delta \hat{a}_1 x_1 + \Delta \hat{a}_2 x_2 + \Delta \hat{a}_3 x_3 + v_s - u \end{cases} \quad (30)$$

To bring these state errors to zero, a sliding surface (s) is defined as follows:

$$s = k_1 e_1 + k_2 e_2 + e_3 \quad (31)$$

where k_1 and k_2 are positive constants. To drive the sliding surface (s) to zero, the cost function and its derivative are considered in Eq. (32) and (33) respectively.

$$V = \frac{1}{2} s^2 \quad (32)$$

$$\dot{V} = s(\dot{s}) \quad (33)$$

Eq. (32) is always positive. To guarantee that the equation will converge to zero when the time goes by (which means that s converges to zero) according to the second method of Lyapunov, Eq. (33) must be negative, which allows Eq. (32) to decrease to zero. Substituting a time derivative of Eq. (31) into (33), leads to

$$\dot{V} = s[k_1 \dot{e}_1 + k_2 \dot{e}_2 + \dot{e}_3] \quad (34)$$

Substituting Eq. (30) into (34) yields

$$\dot{V} = s[k_1 e_2 + k_2 e_3 - \hat{a}_1 e_1 - \hat{a}_2 e_2 - \hat{a}_3 e_3 + \tau_\Delta + v_s - u] \quad (35)$$

where

$$\tau_\Delta = \Delta \hat{a}_1 x_1 + \Delta \hat{a}_2 x_2 + \Delta \hat{a}_3 x_3 \quad (36)$$

τ_Δ can be considered as an uncertain torque caused by residual parameter approximation. To force the system to be asymptotically stable in the sense of Lyapunov, that V is positive and \dot{V} is negative, then the sliding mode control is traditionally proposed in Eq. (37).

$$u = -(\hat{a}_1) e_1 + (k_1 - \hat{a}_2) e_2 + (k_2 - \hat{a}_3) e_3 + v_s + k_{sw} \text{sgn}(s) \quad (37)$$

where

$$k_{sw} \text{sgn}(s) > |\tau_\Delta| \quad (38)$$

The combination of errors as the linear feedback part is to guarantee the system states to stay on the sliding surface (s). The feedback switching part drives sliding surface (s) to zero as quickly as possible. While the feedforward part (v_s) from the input shaping performs sway suppression according to the reference input, if the approximate parameters are close to the actual parameters, the tracking

error will be minimal. The feedback will only need to take care of the mismatched parameters and the external disturbances.

According to Eq. (35) and (37), if s is positive, \dot{s} will be negative, and if s is negative, \dot{s} will be positive. As a result, \dot{V} is always negative. To avoid shattering problem, the signum function (sgn) is traditionally changed to the saturate function (sat), where ε is a small constant preventing shattering phenomena at the sliding surface s near zero:

$$\text{sat}\left(\frac{s}{\varepsilon}\right) = \begin{cases} \text{sgn}\left(\frac{s}{\varepsilon}\right) & \text{if } |s| > \varepsilon \\ \frac{s}{\varepsilon} & \text{else} \end{cases} \quad (39)$$

In Eq. (31), k_1 and k_2 relates the dynamics of the state errors as a second order system, where k_1 and k_2 are interpreted as stiffness and viscosity, respectively. A fast transient response can be achieved by tuning these variables carefully, considering system limitations such as acceleration, deceleration, or even jerk. Using the sat function with a small value of ε , the sliding mode control law contains discrete and continuous part. The switching gain k_{sw} in Eq. (37) can be settled for an appropriate value within the maximum velocity of the overhead crane. It should be high enough to cover the small uncertainty parameters τ_Δ , but not too high to introduce shattering when the sliding surface s close to zero. With the proper parameters, the second method of Lyapunov guarantees stability of the controlled system.

However, the system states are not usually available in practice. Therefore, a state observer must be utilized based on the same model of the overhead crane to observe the states inside the control system. Another advantage of utilizing an observer is the ability to reduce noise in a practical control. A state observer is shown in Eq. (40) where l_1 , l_2 and l_3 are observer gains, tuned by pole placement, \hat{x} is a vector of the estimated states, and $\hat{\theta}$ is the observed output.

$$\begin{cases} \begin{bmatrix} \dot{\hat{x}}_1 \\ \dot{\hat{x}}_2 \\ \dot{\hat{x}}_3 \end{bmatrix} = \begin{bmatrix} 0 & 1 & 0 \\ 0 & 0 & 1 \\ -\hat{a}_1 & -\hat{a}_2 & -\hat{a}_3 \end{bmatrix} \begin{bmatrix} \hat{x}_1 \\ \hat{x}_2 \\ \hat{x}_3 \end{bmatrix} + \begin{bmatrix} 0 \\ 0 \\ 1 \end{bmatrix} u + \begin{bmatrix} l_1 \\ l_2 \\ l_3 \end{bmatrix} (\theta - \hat{\theta}) \\ \hat{\theta} = \begin{bmatrix} 0 & -\hat{c}_2 & 0 \end{bmatrix} \begin{bmatrix} \hat{x}_1 \\ \hat{x}_2 \\ \hat{x}_3 \end{bmatrix} \end{cases} \quad (40)$$

Finally, the model-reference sliding mode control law in Eq. (37) was modified by the estimating errors provided by the observer and the saturate function as follows:

$$u = -(\hat{a}_1) \hat{e}_1 + (k_1 - \hat{a}_2) \hat{e}_2 + (k_2 - \hat{a}_3) \hat{e}_3 + v_s + k_{sw} \text{sat}(\hat{s}) \quad (41)$$

where the estimated errors and the sliding surface are shown below:

$$\begin{cases} \hat{e}_1 = x_{r,1} - \hat{x}_1 \\ \hat{e}_2 = x_{r,2} - \hat{x}_2 \\ \hat{e}_3 = x_{r,3} - \hat{x}_3 \\ \hat{s} = k_1 \hat{e}_1 + k_2 \hat{e}_2 + \hat{e}_3 \end{cases} \quad (42)$$

In this implementation, the feedback control parts (all the terms in Eq. (41) except v_s) should be cut off to zero when the sliding surface s is located around the small gap. Thus, the final control signal u is presented in Eq. (43). According to the dynamic equation of overhead crane in Eq. (24), x_2 linearly relates to the sway angle, and x_1 and x_3 are integral and derivative terms of x_2 , respectively. Therefore, it can be interpreted that if s is a small value, the sway angle is also a small value. Hence, if s is less than a constant λ , the feedback control parts in Eq. (43) is terminated to zero instantly, leaving only the feedforward part v_s .

$$u = \begin{cases} -(a_1) \hat{e}_1 + (k_1 - a_2) \hat{e}_2 + (k_2 - a_3) \hat{e}_3 + v_s + k_{sw} \text{sat}(\hat{s}), & |\hat{s}| > \lambda \\ v_s, & |\hat{s}| < \lambda \end{cases} \quad (43)$$

4. Experiment and Simulation

4.1 Experimental Setup

A 1-ton industrial overhead crane, single girder type was used for verifying the presented input-shaped model reference control. Each axis of the crane is actuated by an AC induction motor and an inverter operated under speed control mode. The crane specification is listed in Table 1.

Table 1. The crane specification for x (girder), y (trolley), and z (hoist) axes, respectively.

Parameters	Values
Travelling spans	23 m, 9 m, 4 m
Maximum velocities	0.36 m/s, 0.33 m/s, 0.13 m/s
Induction motors	0.5 kW, 0.4 kW, 1.8 kW
Crane masses	700 kg, 20 kg, up to 1 ton

However, only the x direction will be tested in this work, which make the overhead unit including the girder, trolley, and hoist mechanisms. An 87-kg payload used in the experiments was heavy enough to make the overhead crane be assumed as a simple-pendulum system.

Figure 5 shows the overhead crane and its components for real implementation. The radio push button sends a user's command signal as a square pulse to PLC to move payload from one point to another. The PLC Omron NX1P2 series is the central processing unit of the control system, which receives the command signal, calculates the control signal, and updates to the inverter for driving the motor. The inverter and the PLC are communicated by a serial communication, Modbus RTU protocol. An MPU-6050, an inertial sensor module contains 3-axis accelerometer and 3-axis gyroscope, is installed on the chain hoisting mechanism for measuring the payload sway angle with a complementary filter for

data fusion. An RF-nano, which is the combination between Arduino Nano and the radio transceiver module (nRF24L01), transmits the sway angle to the PLC via analog converter module with a delay time of 60 milliseconds. The MPU-6050, the RF-nano boards, and batteries are installed on the chain hoist as a wireless sway angle measurement unit, as shown in Fig. 6. A portable computer connects to the PLC by using wireless local area network (WLAN) for collecting data. The control law was implemented on the selected PLC using Sysmac Studio Automation software, which supports international standard PLC language IEC 61131-3.

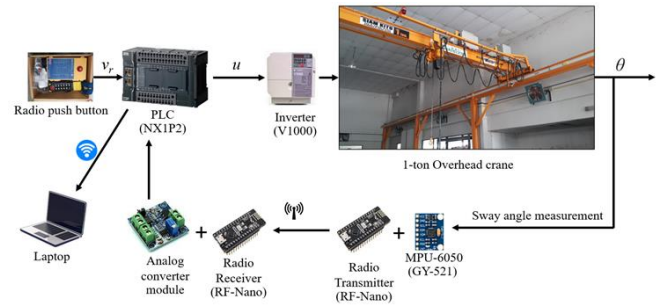


Fig. 5. Hardware overview of the overhead crane.



Fig. 6. Wireless sway angle measurement unit.

Table 2. Parameters of the input-shaped model reference control.

Parameters	Values
A and D	0.36 m/s ² and -0.36 m/s ²
ω and ζ	1.808 rad/s and 0.003
\hat{q} , \hat{l} , and \hat{b}_0	2.5, 3.0 m, and 0.01 s ⁻¹
k_1 , k_2 , and k_{sw}	3.295, 2.51, and 0.07
ε and λ	0.087 and 0.035
l_1 , l_2 , and l_3	1, -2, and -5,
g	9.81 m/s ²

Table 2 expresses the parameters used for the control law and the linear observer in the experiments. Parameters A and D are set as well as acceleration and deceleration limit of the crane. The approximated parameter of the driven unit model, \hat{q} are given as 2.5, based on the acceleration and deceleration limits and default jerk setting.

The sliding model controller parameters were carefully tuned as mentioned before in the previous section. The linear observer gains are manually tuned by considering the reliable sway angle estimation while keeping small observer gains. Then the poles are placed at -2.06 , $-1.06 + 2.48i$, and $-1.06 - 2.48i$. The desired chain length (l), which is selected at 3.0 m, resulting in 1.808 rad/s of the natural frequency (ω). Most the crane operations will happen around these selected values.

For the payload oscillation, the damping ratio (ζ) and the dynamic viscosity (h) were roughly approximated to 0.003 and 0.01 , respectively. The damping ratio was manually obtained by a data fitting, by comparing free response of the measured payload sway and the output of a simple pendulum model, as expressed in Fig. 7. In the figure, the payload was gently pushed by hands and the payload started to oscillate at about the Second 2, which is represented by the black line. The red dashed line is the angular plot of the second order system solution, $\theta_m = Ce^{-h_t/2} \cos(\omega t - \delta)$, where C and δ are arbitrary values. Note that, varying the natural frequency and the payload mass may change the damping ratio and the dynamic viscosity, but with only a tiny difference from the nominal values. Both values can be safely assumed to be constant in the controller design process. Sensitivity analysis by varying natural frequency and the payload mass against the system bandwidth can be seen in the literature [23].

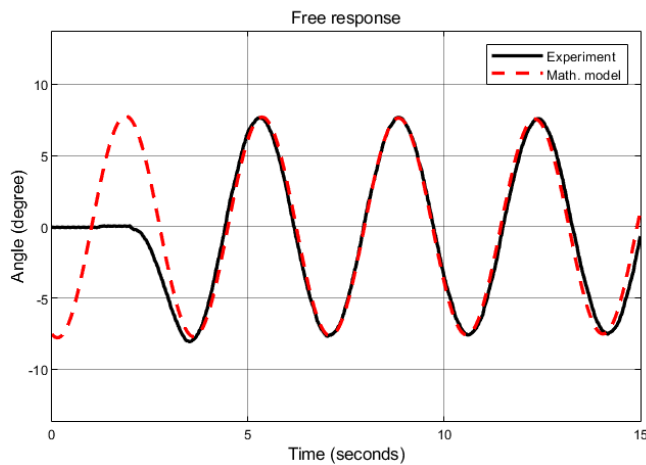


Fig. 7. Parameter estimation of the simple pendulum model.

In this work, the crane position and payload oscillation are considered as the independent variables. Although the presence of the payload sway could affect to the trolley position as expressed in Eq. (9), but in practice, the trolley position is not affected because the overhead crane is driven by the inverter in speed control mode. Given that the inverter power has adequate power, any disturbances such as reaction force from payload sway and the wheel's friction force are compensated by mean of electrical variables, voltage and current. For this reason, the force relation in Eq. (9) is unnecessary, leaving only Eq. (12) in place. To prove this claim, the experimental comparison of the crane position when it is operated

under payload and no payload is provided as shown in Fig. 8, where (a) and (b) are the crane position and the sway angle respectively. In the figure, black line and red dashed line represent the crane with a payload and no payload respectively. For both cases, the crane was commanded by a step-up input at Second 2 to a maximum velocity of 0.36 m/s and step-down at Second 12 to zero velocity. The comparison data confirms that the crane position is not affected by the payload sway oscillation. The deviation of the steady state positions from both cases is about 3 mm from the traveling range of 3.6 m.

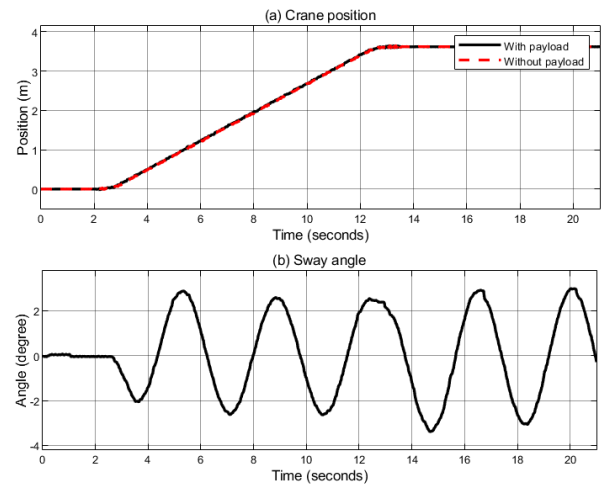


Fig. 8. Experimental result to demonstrate independence between the crane position and payload oscillation variables

4.2 Simulation and Performance Comparison

Before proceeding with the experiments, this subsection provides the simulation result of the presented controller, which is compared to another linear robust control, H infinity design. The controller has ability to confirm the robust stability and the robust performance of the controlled system even it is presented under system uncertainties. Technically, the robust stability means the system is stable in the presence of all types of disturbances, and robust performance means behaviours of the controlled system can be predetermined. According to the robust properties of the H infinity controller, a fair comparison can be made between the presented controller, the input-shaped model reference sliding mode control, and the H infinity control. The H infinity controller is designed by considering the feedback control architecture in Fig. 9 which is the conventional design setup [30].

In this work, w is a reference input, the desired sway angle, of the feedback control loop. P is the generalized controlled system that includes the plant model of the overhead crane and the weighing functions to be defined. z is a performance index that is to be minimized for achieving the transfer function K , the robust controller, where u and y are the input and output of the controlled system, which are the velocity command and the sway angle, respectively. The generalized controlled system is expressed in Eq. (44)

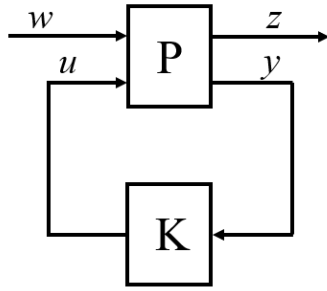


Fig. 9. The conventional system architecture of the H infinity controller.

$$\begin{bmatrix} \tilde{z}_1 \\ \tilde{z}_2 \\ e \end{bmatrix} = \begin{bmatrix} W_s & -W_s G \\ 0 & W_f G \\ I & -G \end{bmatrix} \begin{bmatrix} w \\ u \end{bmatrix} \quad (44)$$

where e is $w - y$. G is the overhead crane model represented in Eq. (23). In the process of designing H infinity control gain, $K(s)$, the selection of the weighing functions $W_s(s)$ and W_f are important. $W_s(s)$ should be a low pass filter or other forms that owns the low pass property. In the same way, $W_f(s)$ should be a high pass filter or other forms that owns the high pass property [31]. The weighing functions that were used in this study are expressed in Eq. (45)

$$W_s(s) = k_{ws} \frac{\omega_s}{s + \omega_s}, \quad W_f(s) = k_{wf} \frac{s}{s + \omega_f} \quad (45)$$

where k_{ws} and k_{wf} are static gains of the low pass filter and the high pass filter, respectively. Setting the static gain k_{ws} and k_{wf} to be high, disturbance rejection and noise attenuation can be expected, respectively. The cut-off frequency of both filters must be carefully tuned. A high ω_s may limit the overshoot response but degrades the disturbance rejection properties. ω_f is the desired system bandwidth [32]. Finally, after formulating the generalized plant in Eq. (44), the MATLAB function “hinfsyn” was used for synthesizing the robust controller transfer function (K). In this study, k_{ws} , k_{wf} , ω_s and ω_f were carefully tuned in the simulation as follows: 100, 10, 0.8, and 20 respectively. The parameters of the plant model G are the same as in Table 2. The synthesized controller according to the H infinity design is shown in Eq. (46)

$$K(s) = \frac{-5.076s^4 - 114.3s^3 - 271.6s^2 - 376s - 830}{s^5 + 9.064s^4 + 40.78s^3 + 105.4s^2 + 62.45s + 0.00014} \quad (46)$$

The simulation was set as shown in Fig. 10. For the fair comparison, the feedforward from the UMZV input shaper is combined with the feedback control signal. The robust stability is confirmed by considering the presence of the noise n , where it is the random numbers between -0.1 and 0.1 degree.

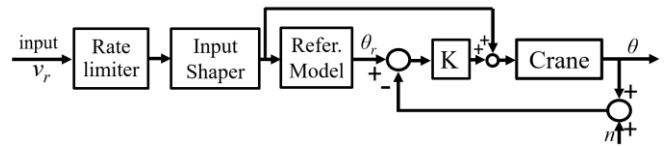


Fig. 10. Diagram of the H infinity control (simulation).

The parameters of the plant model G for simulation, the sliding mode controller, and the UMZV input shaper are provided in Table 2. The simulation setup of the input-shaped model reference sliding mode control is the same as in Fig. 4, where the noise is also added to. The step input (v_r) was used for the emulating input velocity commands when an operator pressing and releasing the push button.

The simulation result of H infinity and sliding mode are shown in Fig. 11 and Fig 12, respectively, where (a) is the input and (b) is the output of the overhead crane. In (a), the black lines represent the case that step input v_r is directly fed to the controlled system without a controller, while the blue lines represent the comparative controllers where the system is set exactly at the known system parameter, which is the chain length of 3 meters. The red and pink lines represent the parameter varying system at the chain lengths of 2.5 and 2.0 meters respectively. From the simulation results, even the two controllers are theoretically considered as robust control techniques, the performance provided by the sliding mode control is clearly better based on the controlled system setup. Although, the H infinity demonstrates the robustness against the parameter varying but many overshoots occurred when system parameters were changed. Meanwhile, the overshoot responses of the sliding mode are almost not found. Moreover, the similar results can be found in the literature [33], where the oscillatory base manipulator was studied. However, tuning the weighing functions of the H infinity relies on the frequency domain, which relates to the selected functions and parameters. Therefore, achieving a good transient response by tuning the functions would be difficult. Based on the simulation results in this work, the sliding mode provides more robust performance than the H infinity control.

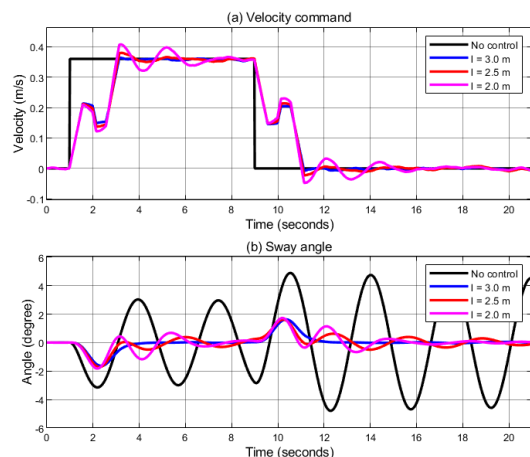


Fig. 11. The H infinity control responses from the simulation at various chain lengths.

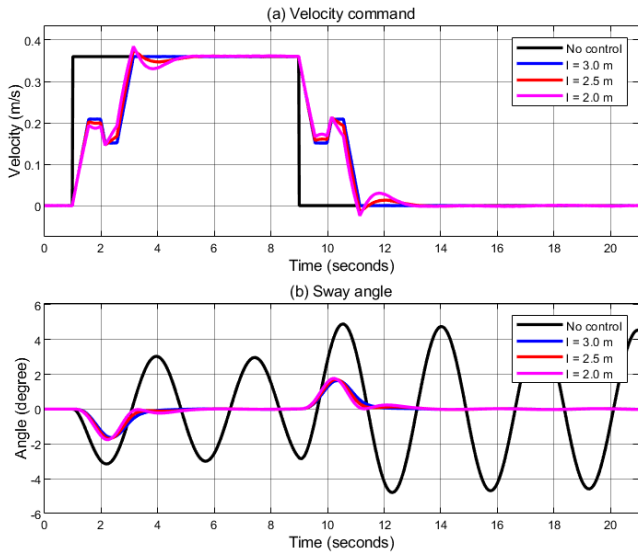


Fig. 12. The sliding mode control responses from the simulation at various chain lengths.

4.3 Experimental Results

To test the effectiveness of the presented control system, the control system was tested in two scenarios: tracking and regulator modes. In tracking mode, the reference or command velocity (v_r) signal is set to step up at Second 2 and step down at Second 12, which mimics the user pressing and releasing the radio push button at these times. The command amplitudes were at the maximum velocity of 0.36 m/s when pressing, and at zero velocity when releasing. The PLC calculated the processed velocity command u according to the input-shaped model reference control in Eq. (43). The processed velocity command was bounded for the maximum velocity of the overhead crane (0.36 m/s) and mapped to the maximum electrical frequency supply of the inverter, which is 50 Hz. The inverter was operated in the speed control mode, which receives the velocity commands from the PLC. The acceleration and deceleration limits were set at 0.36 m/s² along with the default jerk setting. The experiments were carried for 4 cases as follows:

Case 1 The chain length was fixed at 3 meters ($l = \hat{l} = 3$), and the input-shaped model reference control was designed at this exact length.

Case 2 The chain length was fixed at 2 meters ($l = 2$), while the UMZV input shaper was designed at 3 meters ($\hat{l} = 3$) to test the effect of the parameter variation. In this case, the model reference sliding mode control was expected to handle the residual vibration caused by the UMZV input shaper due to the mismatched design.

Case 3A is similar to the Case 2 but instead the chain length was fixed at 3.8 m ($l = 3.8$, $\hat{l} = 3$), which resulted in a lower natural frequency.

Case 3B has the same parameters as the Case 3A, except the velocity command (v_r) is longer and has more impulses than the previous 3 cases. This case is for demonstrating

effects of a long operation when the push button is frequently pressed and released over the time.

From the experiments, the performance comparisons of the Case 1, 2, 3A, and 3B are shown in Fig. 13, Fig. 14, Fig. 15, and Fig. 16, respectively. In these figures, the velocity command graph is denoted by (a) and the sway angle graph is denoted by (b). In each graph, the velocity commands and the sway angles are compared by varying controller types: No control, the UMZV input shaper, and the hybrid (input-shaped model reference control), represented by black lines, red lines, and blue lines, respectively.

For Case 1, the UMZV input shaper provided an effective payload sway suppression. The parameters of both the controlled system and the feedforward control including natural frequency, damping ratio, and both acceleration and deceleration limits are precisely matched. The result demonstrated that the input shaper works well for sway suppression when the chain length, the acceleration, the deceleration, and the damping ratio are well known. From Fig. 13, the residual vibration after Second 12 was below 0.1 degree, compared with 3.2 degree by the “no control” signal (that is 96% of vibration suppression). In this case, both the input shaper and the model reference control functioned well. The feedforward control signal was lightly perturbed by the feedback control signal due to small parameter approximation errors in the real-world experiment.

From the experimental result of Case 1 in Fig. 13, the command from the hybrid control differed from the UMZV after the step-down input at Second 12 because the parameter approximation error accumulated over time. Especially, the correcting signal provided by the feedback control was actuated after the push button was released (Second 13 and 15). As described, the residual sway angle tends to increase when the number of open-loop signal increases, even with the input shaping, which small parameter approximation error can accumulate over time. Thus, it explains that why the feedback control (in hybrid) tried to correct the feedforward signal only after the step-down input (releasing push button).

For Case 2 and 3A, the sway suppression provided by the UMZV input shaper was degraded due to the large parameter approximation error, which the feedforward control is naturally sensitive to. The natural frequency in the shaper design was deviated from the actual plant system for +22% and -11% in both cases respectively. In Fig. 14, the residual sway angle at Second 15 was reduced from 6.0 (no control) to 2.5 degree (UMZV). That was 61% of vibration suppression for Case 2. Similarly, in Case 3A, the sway angle was reduced from 4.5 to 1.2 degree (73% of vibration suppression) at Second 15 to 17, as shown in Fig. 15.

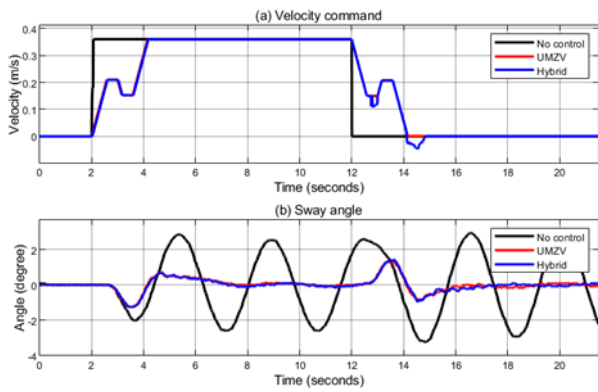


Fig. 13. Performance comparison for Case 1 (3.0 m of chain length).

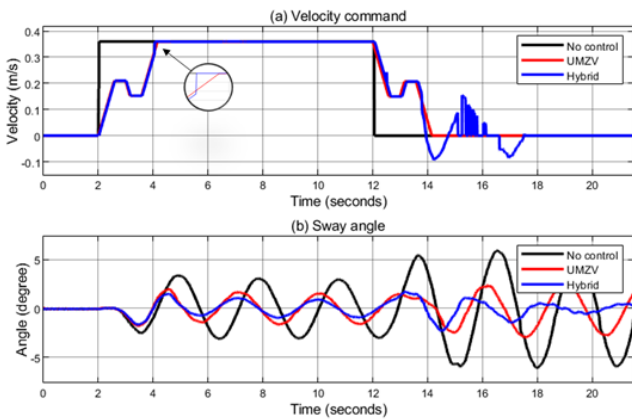


Fig. 14. Performance comparison for Case 2 (2.0 m of chain length).

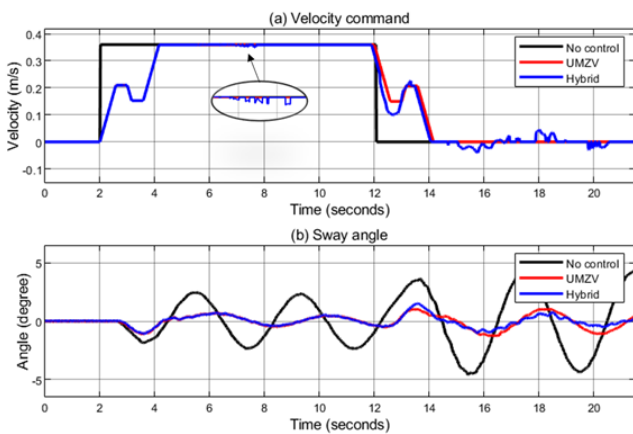


Fig. 15. Performance comparison for Case 3A (3.8 m of chain length).

The hybrid commands further improved the sway suppression for both Case 2 and 3A. After the push button was released, the feedback control using model-reference sliding mode control tried to correct the feedforward signal until the sliding surface s was close to zero, that is $s < \lambda$. However, according to the measurement from Fig. 14 and Fig. 15, the residual sway angles were about 0.5 degree, which equates to suppression performance of 92% and 88% respectively, with respect to the no control. For the control effort aspect, the feedback control was first active at Second 4 in Case 2

(Fig. 14), and Second 7 in Case 3A (Fig. 15), which reduce the sway angle of the hybrid control as compared to the UMZV. Note that the result of Case 3A shows little improvement in sway suppression for the Hybrid (0.5 degree) compared to the UMZV (1.2 degree). But the sway suppression will be significantly improved with a longer velocity command.

In general, any feedforward control signals induce the payload oscillation, even with the input shaping signal due to parameter approximation error in practice. Moreover, if the crane is frequently commanded by a large number of impulses, like in a normal operation where the operator arbitrarily pressing and releasing the pendant buttons, residual oscillation will be larger from accumulation. In this case, the performance of the feedforward control, UMZV, must be lower than the those from the 3 previous experiments, where only 2 impulses were used. Meanwhile, the suppression performances of the Hybrid are certainly higher due to the feedback control nature. In short, if the number of impulses increase, the performance of the UMZV will be lower, and the Hybrid will be higher. Therefore, the Case 3B was tested with the same parameters as Case 3A except with an increased number of impulses. The crane was commanded to perform the start-stop motion for 6 times, alternately forward and reverse directions (total of 12 impulses). Each start-stop period is set for 5 seconds and each movement is delayed for 5 seconds. The results of the Case 3B are shown in Fig. 16.

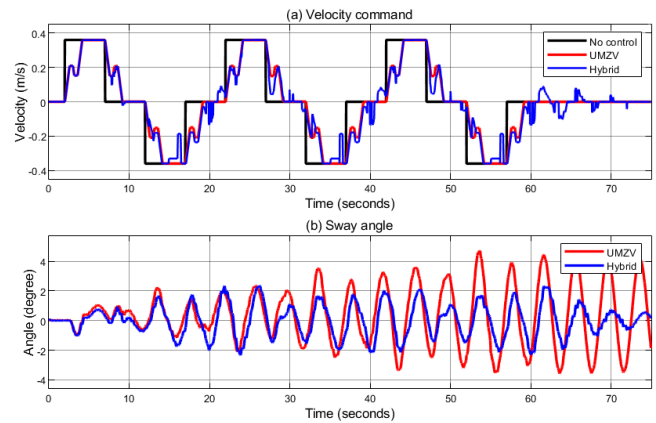


Fig. 16. Performance comparison for Case 3B (same as Case 3A, but with an increased number of impulses).

In Fig. 16, the feedback control in the Hybrid tried to correct the residual from the UMZV command, resulting in the final residual oscillation (Second 75) of 0.5 degree. Meanwhile UMZV induced the final residual value of 4.2 degree. Note that the payload sway response of the “no control” case cannot be reported because of a dangerously large sway motion, thus the test was terminated. Table 3 summarizes the residual sway angles and suppression performances of the four cases using the three controllers.

Table 3. Summary of the residual sway angles and suppression performances of the controllers from the experiments.

Cases	No control	UMZV	Hybrid
1	3.2°	0.1° (96% improved)	0.1° (96% improved)
2	6.0°	2.5° (61% improved)	0.5° (92% improved)
3A	4.5°	1.2° (73% improved)	0.5° (88% improved)
3B	-	4.2°	0.5°

Figure 17 shows the performance of the input-shaped model reference control, operated as a regulator when the reference velocity was not sent to move the crane, but non-zero initial sway angle was introduced. The chain length was fixed at 3.0 meters along with the acceleration and deceleration limit of 0.36 m/s² (similar to Case 1). The payload was pushed by hands at Second 3 (red line) intending to mimic a perturbation in a disturbance situation. The feedback sway control was activated at Second 9 (blue line), the crane was moved according to control law trying to push all system states to zero. The sway angle became close to zero, at about 0.5 degree by measurement at Second 18.

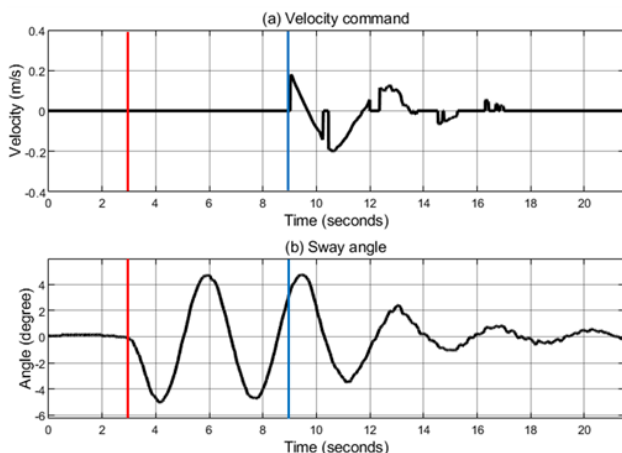


Fig. 17. Sway suppression in the regulator mode.

5. Conclusion

This paper showed the implementation of the input-shaped model reference control for the industrial overhead crane. The UMZV input shaper and the model-reference control based on the sliding design were combined as a hybrid control. These two control laws work well together for sway suppression. The input shaper shapes original command to cancel residual vibration, while the feedback control takes care of parameter variation and non-zero initial sway angle. The comparison of the proposed hybrid control with another feedback controller, H infinity, for benchmarking is also provided via simulation, which the sliding mode control provides

the better response results. State tracking control and state regulator were demonstrated experimentally.

In the tracking control mode, the results showed that both the UMZV input shaper and the model-reference sliding mode control work well when the overhead crane operated at a desired condition. The hybrid controller can operate better than UMZV under parameter variations such as different chain length, which degrades suppression performance of the UMZV input shaper. The feedback control assists the feedforward by correcting the feedforward signal, trying to force the system states to desired states of the reference model. This controller form allows feedback and feedforward control to work harmoniously according to model-reference control form. Moreover, the sliding mode control was also tested for its suppression performance in the regulator mode, in which the feedforward UMZV signal was not sent to the control system and the initial non-zero sway was introduced. By the experiment, the sway angle amplitude was reduced to a small value closed to zero, which was determined by the hybrid control command.

In conclusion, the input-shaped model reference control is a suitable choice for industrial crane applications. The input-shaped model reference control provides satisfactory performances as not only the trajectory tracking control but also the regulator as demonstrated in this paper.

Acknowledgement

This research was partly funded by Siam Kito Co., Ltd, Thailand. We honestly thank Siam Kito Co., Ltd. for their technical supports and valuable advice from their expertise in the field.

References

- [1] L. Ramli, Z. Mohamed, A. M. Abdullahi, H. I. Jaafar, and I. M. Lazim, "Control strategies for crane systems: A comprehensive review," *Mechanical Systems and Signal Processing*, vol. 95, pp. 1-23, Oct. 2017.
- [2] M. J. Maghsoudi, Z. Mohamed, M. O. Tokhi, A. R. Husain, and M. S. Z. Abidin, "Control of a gantry crane using input-shaping schemes with distributed delay," *Transactions of the Institute of Measurement and Control*, vol. 39, no. 3, pp. 361-370, 2017.
- [3] T. Vyhlídal, V. Kucera, and M. Hromčík, "Signal shaper with a distributed delay: Spectral analysis and design," *Automatica (Journal of IFAC)*, vol. 49, pp. 3484-3489, 2013.
- [4] V. D. La and K. T. Nguyen, "Combination of input shaping and radial spring-damper to reduce tridirectional vibration of crane payload," *Mechanical Systems and Signal Processing*, vol. 116, no. 3, pp. 310-321, 2019.
- [5] A. Mohammed, K. Alghanim, and M. T. Andani, "An adjustable zero vibration input shaping control

- scheme for overhead crane systems,” *Shock and Vibration*, vol. 2020, no. 3, pp. 1-7, 2020.
- [6] A. Alfadhli and E. Khorshid, “A smooth optimized input shaping method for 2D crane systems using Bezier curves,” *Transactions of the Institute of Measurement and Control*, vol. 43, no. 11, pp. 2512-2524, 2021.
- [7] A. M. Abdullahi, Z. Mohamed, M. S. Z. Abidin, S. Buyamin, and A. A. Bature, “Output-based command shaping technique for an effective payload sway control of a 3D crane with hoisting,” *Transactions of the Institute of Measurement and Control*, vol. 39, no. 10, pp. 1443-1453, 2017.
- [8] A. M. Abdullahi, Z. Mohamed, H. Selamat, H. R. Pota, M. S. Z. Abidin, F. S. Ismail, et al, “Adaptive output-based command shaping for sway control of a 3D overhead crane with payload hoisting and wind disturbance,” *Mechanical Systems and Signal Processing*, vol. 98, pp. 157-172, 2018.
- [9] B. Lu, Y. Fang, and N. Sun, “Sliding mode control for underactuated overhead cranes suffering from both matched and unmatched disturbances,” *Mechatronics*, vol. 47, pp. 116-125, 2017.
- [10] X. Gu and W. Xu, “Moving sliding mode controller for overhead cranes suffering from matched and unmatched disturbances,” *Transactions of the Institute of Measurement and Control*, vol. 44, no. 1, pp.60-75, 2022.
- [11] H. X. Le, A. V. Le and L. Nguyen, “Adaptive fuzzy observer based hierarchical sliding mode control for uncertain 2D overhead cranes,” *Cyber-Physical Systems*, 2019.
- [12] V. A. Le , H. X. Le, L. Nguyen, and M. X. Phan, “An efficient adaptive hierarchical sliding mode control strategy using neural networks for 3D overhead cranes,” *International Journal of Automation and Computing*, vol. 16, no. 5, pp. 614-627, Oct. 2019.
- [13] H. Ouyang, J. Wang, G. Zhang, L. Mei, and X. Deng, “Novel adaptive hierarchical sliding mode control for trajectory tracking and load sway rejection in double-pendulum overhead cranes,” *IEEE Access*, vol. 7, no. 3, pp. 10353-10361, 2019.
- [14] H. V. Pham, Q. Hoang, M. V. Pham, D. M. Do, N. H. Phi, etc., “An efficient adaptive fuzzy hierarchical sliding mode control strategy for 6 degrees of freedom overhead crane,” *Electronics*, vol. 11, no. 5, 2022.
- [15] M. Zhang, Y. F. Zhang, and X. Cheng, “An enhanced coupling PD with sliding mode control method for underactuated double-pendulum overhead crane systems,” *International Journal of Control, Automation and Systems*, vol. 17, no. 6, pp. 1579-1588, 2019.
- [16] A. M. Abdullahi, Z. Mohamed, H. Selamat, H. R. Pota, M. S. Z. Abidin, and S. M. Fasih, “Efficient control of a 3D overhead crane with simultaneous payload hoisting and wind disturbance: design, simulation and experiment,” *Mechanical Systems and Signal Processing*, vol. 145, no. 3, pp. 1-16, 2020.
- [17] D. Fujioka and W. Singhose, “Control effort reduction analysis of zero-vibration model reference control for controlling a time-varying plant,” in *American Control Conference (ACC)*, Portland, Oregon, USA, 2014, pp. 3110-3115.
- [18] D. Fujioka, M. Shah, and W. Singhose, “Robustness analysis of input-shaped model reference control on a double-pendulum crane,” in *Proceedings of the American Control Conference*, Chicago, IL, USA, 2015, pp. 2561-2566,
- [19] D. Fujioka and W. Singhose, “Performance comparison of input-shaped model reference control on an uncertain flexible system,” *IFAC-PapersOnLine*, vol. 48, no. 12, pp. 129-134, 2015.
- [20] D. Fujioka and W. Singhose, “Input-shaped model reference control of a nonlinear time-varying double-pendulum crane,” presented at *10th Asian Control Conference (ASCC)*, 31 May-3 June 2015.
- [21] H. Jaafar, Z. Mohamed, M. A. Ahmad, N. A. Wahab, L. Ramli, and M. H. Shaheed, “Control of an underactuated double-pendulum overhead crane using improved model reference command shaping: Design, simulation and experiment,” *Mechanical Systems and Signal Processing*, vol. 151, 2021.
- [22] Q. Hu and W. Xu, “AUDE-based model reference adaptive dynamic sliding mode control for overhead cranes,” *International Core Journal of Engineering*, vol. 8, no. 4, 2022.
- [23] M. Ermidoro, A. L. Cologni, S. Formentin, and F. Previdi, “Fixed-order gain-scheduling anti-sway control of overhead bridge cranes,” *Mechatronics*, vol. 39, pp. 237-247, 2016.
- [24] K. L. Sorensen, W. Singhose, and S. Dickerson, “A controller enabling precise positioning and sway reduction in bridge and gantry cranes,” *Control Engineering Practice*, vol. 15, no. 7, pp. 825-837, 2007.
- [25] N. Suksabai, J. Waikoonvet, and I. Chuckpaiwong, “Modelling method investigation of drive and motor for an industrial overhead crane,” *IOP Conference Series: Materials Science and Engineering*, vol. 886, p. 012030, 2020.
- [26] Y. Mori and Y. Tagawa, “Vibration controller for overhead cranes considering limited horizontal acceleration,” *Control Engineering Practice*, vol. 81, pp. 256-263, 2018.
- [27] W. E. Singhose, W. P. Seering, and N. C. Singer, “Time-optimal negative input shapers,” *Journal of Dynamic Systems, Measurement, and Control*, vol. 119, no. 2, pp. 198-205, 1997.
- [28] S. Gürleyük, “Optimal unity-magnitude input shaper duration analysis,” *Archive of Applied Mechanics*, vol. 77, pp. 63-71, 2007.
- [29] R. Piedrafita, D. Comín, and J. R. Beltrán, “Simulink® implementation and industrial test of Input Shaping techniques,” *Control Engineering Practice*, vol. 79, pp. 1-21, 2018.
- [30] H. Kwakernaak, “Robust control and H_∞ -optimization—Tutorial paper,” *Automatica*, vol.29, no. 2, pp. 255-273, 1997.

- [31] N. Dey, U. Mondal, and D. Mondal, "Design of a H-infinity robust controller for a DC servo motor system," in *2016 International Conference on Intelligent Control Power and Instrumentation (ICICPI)*, 2016, pp. 27-31.
- [32] H. Ali, S. Noor, S. M. Bashi, and M. H. Marhaban, "Design of H-inf controller with tuning of weights using particle swarm optimization method," *LAENG International Journal of Computer Science*, vol.38, no. 2, pp. 103-112, 2011.
- [33] R. Koshy and P. R. Jayasree, "Comparative study of H-infinity and sliding mode control for a manipulator with oscillatory-base," *2017 International Conference on circuits Power and Computing Technologies [ICCPCT]*, 2017, pp. 1-6.



Nattapong Suksabai was born in Bangkok, Thailand in 1992. He received M.Eng. in Mechanical Engineering from Mahidol University, Thailand in 2017. He is now pursuing Ph.D. degree in Mechanical Engineering at Mahidol University. His research interests include active vibration suppression system and control system design.



Ittichote Chuckpaiwong received the M.S. degree in Systems and Control Engineering from Case Western Reserve University in 2001, and Ph.D. degree in Mechanical Engineering from Georgia Institute of Technology, Atlanta in 2003. His research interests include smart crane systems, cable driven parallel robots, adaptive signal processing, Internet of Things and mechatronics systems.